processes

MDPI

Article

Olive Mill by-Products Thermochemical Conversion via Hydrothermal Carbonization and Slow Pyrolysis: Detailed Comparison between the Generated Hydrochars and Biochars Characteristics

Ahmed Amine Azzaz [1,2], Camélia Matei Ghimbeu [1,2], Salah Jellai [3], Leila El-Bassi [4] and Mejdi Jeguirim [1,2,*]

[1] CNRS, Institut de Science des Matériaux de Mulhouse (IS2M) UMR 7361, Université de Haute-Alsace, F-68100 Mulhouse, France; amine.azzaz@uha.fr (A.A.A.); camelia.ghimbeu@uha.fr (C.M.G.)
[2] CNRS, Institut de Science des Matériaux de Mulhouse (IS2M) UMR 7361, Université de Strasbourg, F-67081 Strasbourg, France
[3] Centre for Environmental Studies and Research (CESAR), Sultan Qaboos University, Al-Khoud 123, Muscat, Oman; s.jelali@squ.edu.om
[4] Laboratory of Wastewater and Environment, Center of Water Research and Technologies (CERTE), Borj Cedria Ecopark, P.B. 273, Soliman 8020, Tunisia; l.elbassi@gmail.com
* Correspondence: mejdi.jeguirim@uha.fr; Tel.: +33-(0)3-89-33-67-29

Abstract: In this research work, an ecofriendly approach was adopted for the treatment of two abundant liquid and solid agricultural wastes generated by olive mill industry: olive mill wastewater (OMWW) and raw olive pomace (ROP). It consists, firstly of the impregnation of ROP by OMWW and the conversion of the resulting impregnated sample (IROP) into hydrochars and biochars through hydrothermal carbonization (HTC) and slow pyrolysis methods, respectively. The impact of the treatment temperature on the physico-chemical properties of the derived chars was assessed by various analytical techniques. The hydrochars production yields were found to be higher than the biochars ones and associated to the lower temperature used. However, the generated biochars possess higher carbon percentage and lower volatile matter contents. In addition, the increase of the hydrothermal and pyrolysis carbonization temperatures shows an increase of macro-elements contents and a significant decrease of the O/C ratios which led to an enhancement of the high heating value for both hydrochars and biochars. The FTIR and Boehm titration analysis highlighted a significant alteration of the biochars surface chemistry compared to hydrochars evidenced by the lower amount of functional groups. The collected data emphasize on the efficient potential application of hydrochars and biochars for agricultural and environmental applications, respectively. Furthermore, it was noted that both chars have high energetic potentials and could be used for co-firing with coal in industrial boilers.

Keywords: hydrothermal carbonization; pyrolysis; olive mill wastewater; olive pomace; structural characterization

Citation: Azzaz, A.A.; Matei Ghimbeu, C.; Jellai, S.; El-Bassi, L.; Jeguirim, M. Olive Mill by-Products Thermochemical Conversion via Hydrothermal Carbonization and Slow Pyrolysis: Detailed Comparison between the Generated Hydrochars and Biochars Characteristics. *Processes* **2022**, *10*, 231. https://doi.org/10.3390/pr10020231

Academic Editor: Albert Ratner

Received: 20 December 2021
Accepted: 23 January 2022
Published: 25 January 2022

1. Introduction

During the last century, the agri-food industry played a very important role in the development of agriculture related sectors [1]. Indeed, the processing industry for extensively consumed agricultural products such as cereals, vegetables, fruits, animal-source products, and oils occupies an important place in worldwide economies and especially in developing countries [2]. The majority of these industries generate various wastes that have to be seriously taken into consideration in order to avoid any negative effects on the environment and human health [3].

Consequently, the sustainable management of agri-food industry wastes presents very interesting valorization potentials in agricultural, environmental and energetic sectors [4,5].

Various studies investigated these wastes for targeted molecules extraction [6–9], biopolymers synthesis [10,11], fabrication of electrodes for energy storage systems such as batteries and supercapacitors [12,13] or highly porous media for air or water treatment [14–16]. Among the diverse valorization techniques of these agricultural wastes, the slow pyrolysis and hydrothermal carbonization received great attention for the synthesis of value-added and carbon rich materials, named biochars and hydrochars, respectively. These generated byproducts have interesting characteristics that allow them to be valorized in numerous application fields [17–20].

Slow pyrolysis, as a classical carbonization method, was widely employed for the conversion of organic wastes into materials with very high carbon and low volatile matter contents [21]. Along with the solid biochar, these feedstocks transformation at inert atmosphere produced two other carbonization by-products, i.e., syngas and bio-oil, that are known for their interesting energetic properties [22]. A significant attention is attributed to the biochar upgrading into more interesting carbon material with very specific characteristics through targeted physical, chemical and/or thermal activation depending on the final desired application [18,23]. Few drawbacks were noted when opting for this technique concerning mainly: (i) the relatively high energy consumption related to the high pyrolysis temperatures (350 °C–750 °C), (ii) the pre-drying step for feedstocks containing high moisture percentage and (iii) the relatively low final solid yield at high temperatures [24]. Hydrothermal carbonization, on the other hand, has recently emerged as a very promising and non-polluting method for the conversion of organic resources into early-carbon materials with specifically tuned characteristics [17]. The carbonization process is performed in a liquid medium, transformed into a subcritical fluid under the effect of temperature (150–350 °C) and autogenetic pressure, thus reducing significantly the energetic consumption [25]. It has been also reported that hydrothermal carbonization reduces the content in minerals in the solid residues, which could be considered as an interesting method for impurities removal [26].

In the Mediterranean region, olive oil production industry generally generates significant amounts of both ROP and OMWW [27]. The sustainable management of these wastes has become an urgent issue due to their proved negative effects on the environment [28]. The slow pyrolysis and hydrothermal carbonization applications for these olive mill wastes conversion into carbonaceous materials has been carried out at lab scale under various experimental conditions [26,29]. However, to the best of our knowledge, there were no research works that focused on the comparison between the physico-chemical properties of the generated biochars and hydrochars from the IROP.

Therefore, the main aim of this study is to synthetize and deeply characterize the generated hydrochars and biochars under different experimental conditions of hydrothermal carbonization and slow pyrolysis of the impregnated olive pomace with OMWW. The focus was mainly on the comparison of their physico-chemical characteristics with the aim of evaluating their potential applicability in different fields.

2. Materials and Methods

2.1. Raw Feedstock Collection and Preparation

Raw olive pomace (ROP) was collected from a local three phase milling plant in the region of Touta, Northeast of Tunisia. Afterwards, this light brown lignocellulosic solid waste was dried in ambient air then stocked in airtight bags then exposed periodically to ambient air in order to avoid any possible chemical/biological modification. Olive mill wastewater (OMWW) was provided from the same olive oil plant. It was stored in cans at low temperature (<4 °C). Both ROP and OMWW were used in the following experiments without any performed treatments or purifications. The ROP was impregnated with OMWW in batch reactor according to the protocol detailed by Bargaoui et al. [30]. Briefly, 40 g of ROP were stirred in 200 mL of OMWW by using a mechanical stirrer for 4 h at a stirring speed of 300 rpm. The resulting solid was afterwards dried at 60 °C overnight and named Impregnated Raw Olive Pomace (IROP).

2.2. Carbonization Process

The carbonization was performed using two approaches, namely, hydrothermal carbonization and slow pyrolysis.

2.2.1. Hydrothermal Carbonization

Hydrochars were prepared as follows: deionized water was added to IROP at a ratio of 9:1 (g of deionized water: g of solid feedstock). The mixture was then inserted in a 100 mL high pressure autoclave (Top Industrie, Vaux-le-Pénil, France), and the effect of temperature was monitored at 180, 200 and 220 °C using a programmable oven (Memmert, Schwabach, Germany). The heating rate and residence time were fixed for all the experiments to 10 °C/min and 24 h, respectively. Afterwards, the related mixtures were vacuum filtered using 0.45 µm Whatmann® filter paper (VWR, Leuven, Belgium) in order to separate the carbonaceous solid from the liquid phase. The resulting hydrochar was dried overnight at 60 °C and then stocked in glass vials for subsequent use.

2.2.2. Slow Pyrolysis Carbonization

The biochar production was performed as follows: 3 g of IROP were placed in an alumina crucible and introduced in tubular furnace reactor. Then, argon flow was supplied continuously at room temperature during 30 min in order to remove residual oxygen. Next, the temperature was increased to the setting values (i.e., 400, 500 and 600 °C) with a heating rate of 5 °C/min under argon at a flow rate of 6 N L/h. The sample was maintained during 1 h at the desired temperature and then cooled naturally under argon flow.

The produced hydrochars and biochars were then stocked in glass vials for further use. Samples were thereby named as follows: T-IROP where T stands for the process temperature (°C). All experiments were performed in triplicates, and standard deviation of the results was set to ±3%.

2.3. Chars Characterization

2.3.1. Solid Yield Determination

The solid yields (Y_{HC}; %) for both carbonization processes were determined according to the following formula:

$$Y_{HC}(\%) = m_{HC}/m_{FS} \times 100 \quad (1)$$

where m_{HC} (g) is the recovered dry solid mass after carbonization, and m_{FS} is the initial feedstock mass (g).

2.3.2. Physico-Chemical Characterization of the Produced Hydrochars and Biochars

Proximate, Ultimate and Mineral Composition Analysis

Proximate analysis was performed for all biomass derived chars in order to determine their contents in volatile matter, fixed carbon and ash. The thermogravimetric analysis (TGA) was conducted according to the experimental protocol enunciated in our previous work [29]. The determination of macro elements was achieved using two different techniques. The content in *C*, *H*, *N* and *S* for hydrochars and biochars was assessed using a Flash 2000 CHNS-O elemental analyzer (Thermo Scientific, Cambridge, UK). The content in oxygen was deduced by difference as follows:

$$O(db.\%) = 100 - (Ash\ (db.\%) + C\ (db.\%) + H\ (db.\%) + N\ (db.\%) + S\ (db.\%)) \quad (2)$$

The amount of minerals was investigated with two different methods for the two types of chars. Hydrochars mineral content was determined according to the Thomson and Leege method which was detailed in our previous paper [26,31]. As for biochars, the content in elements including K^+, Na^+, Mg^{2+} and Ca^{2+} was determined through X-ray fluorescence. Generally, 200 mg of biochar mixed with 100 mg of boric acid (used as a binder) and then pressed to form a pellet which was analyzed using spectrophotometry by a PHILIPS PW2540 (Amsterdam, Netherlands) apparatus with a rhodium target X-ray tube.

The content in C and O previously determined by the elemental analyzer were used for the calibration of the XRF specters and the determination of the given minerals' concentrations.

Structure and Morphology

X-ray diffraction (XRD) analysis was used on both types of chars to determine their crystalline structure. The study was performed using a Panalytical X'Pert powder diffractometer (Malvern, UK) equipped with a copper anode. The resulting diffractograms were analyzed using X'Pert Highscore software, and the crystalline peaks were identified by means of the international center for diffraction data (ICDD) database. The morphology of hydrochars and biochars was determined through Scanning electronic microscopy (SEM) analysis using a XL30 electron microscope (Philips, Eindhoven, The Netherlands).

Surface Chemistry

The bulk quantitative characterization of the produced chars was performed with three methods. Firstly, pH at zero-point-charge (pH_{ZPC}) was determined to estimate the dominating surface charge. Then, acidic and basic groups quantification was done using the Boehm titration method. Both methodologies were described thoroughly in the literature [29,32]. The surface chemistry was also assessed using the Fourier transform infrared spectroscopy (FTIR). Acquisition of the FTIR spectra was performed with an Equinox 55 Brucker spectrometer (Ettlingen, Germany). For each sample, an exact biochar/hydrochar mass to KBr ratio of 1/200 was ground in a mortar and pressed into 1 cm diameter disk with 3.5 tons pressure. The disk-like sample was then analyzed at a spectral resolution of 4 cm^{-1}, measured between 4000 cm^{-1} and 400 cm^{-1}.

Energy Content

In order to evaluate the energetic capacity of the produced biochars/hydrochars heir high heating value (HHV) was quantified using an IKA C200 bomb calorimeter (Staufen, Germany). The experiment was performed according to DIN 51900 [33] at isoperibolic reaction mode and following the protocol detailed in our previous papers [26,29].

3. Results

3.1. Carbonization Yield and Proximate Analysis

The temperature effect on the final chars yields is presented in Figure 1. It can be remarked that the final yield presents different tendencies between the two types of carbonaceous materials. In fact, the final hydrochars yields ranged between 56% and 42% for temperatures between 180 °C and 220 °C, respectively (Figure 1). These yields are in agreement with the values reported in previous papers investigating the hydrothermal carbonization of biomasses [34,35]. On the contrary, the biochars produced at temperatures between 400 °C and 600 °C revealed a rather constant final solid yield varying between 36% and 38%, respectively. The increase in carbonization temperature generally lead to an increase in heat transfer to the inner material which increases the conversion rate of organic material into a more stable structure [36]. The carbonization of the non-impregnated ROP previously performed by Azzaz et al. [26] and Marks et al. [27] using hydrothermal carbonization and slow pyrolysis under similar experimental conditions showed final yields between 55% and 38% for hydrochars and between 38% and 30% for biochars, respectively. The difference in final yields is clearly in favor of the impregnated biomass suggesting that the impregnation of OMWW increased the feedstocks' content in organic material which eventually will enhance their final solid mass.

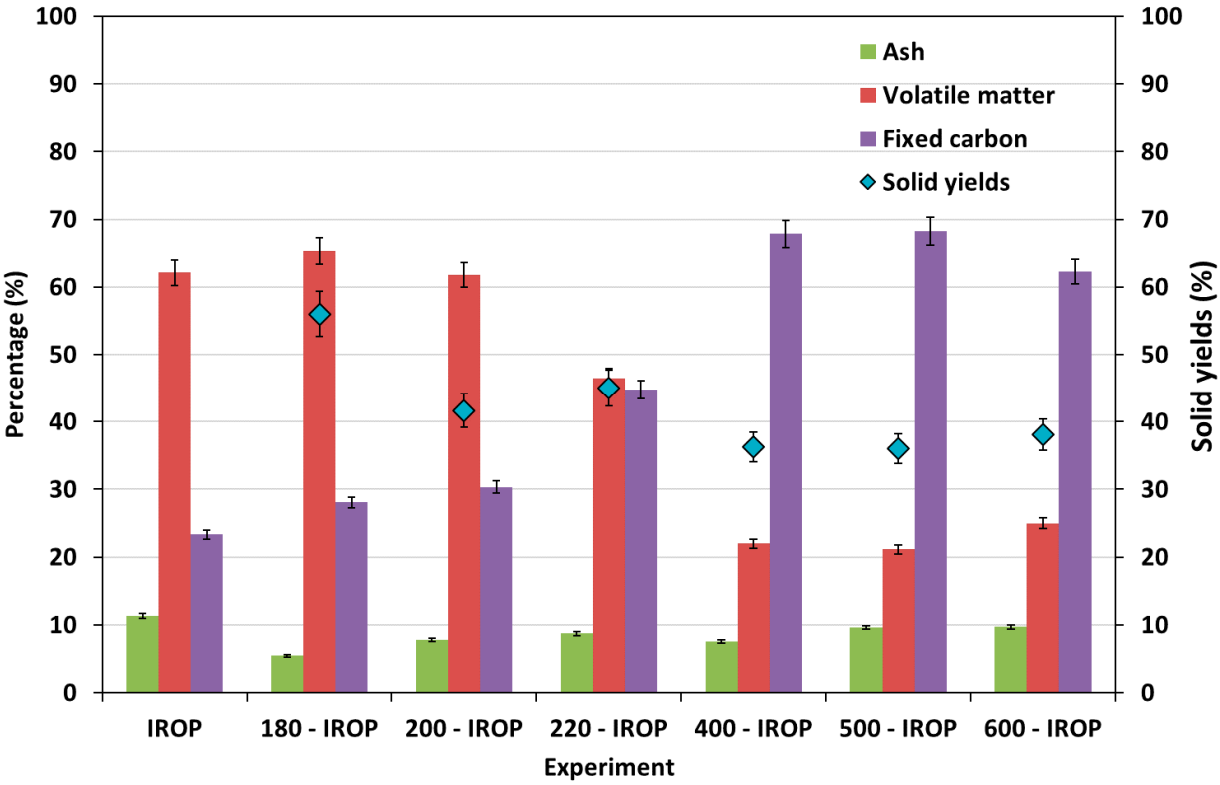

Figure 1. Solid production yields and proximate analyses of hydrochars and biochars produced from impregnated IROP under different temperatures and processes.

These results were further confirmed by proximate analysis, presented in Figure 1. Initially, the impregnated olive pomace is characterized by volatile matter, fixed carbon and ash contents of 62%, 23% and 11%, respectively. Similar observations were reported by Jeguirim et al. [37], when investigating the impact of OMWW impregnation onto sawdust at an OMWW/sawdust ratio of 5:1.

The IROP carbonization using two techniques led to similar tendencies in terms of proximate composition but with different rates. The hydrothermal carbonization increased significantly the content in fixed carbon from 23% for IROP to 45% for 220-IROP, respectively. The opposite tendency was noticed for volatile matter which decreased from 62% to 46% for the same samples. On the other hand, the fixed carbon content significantly increased when performing slow pyrolysis reaching about 62% whereas the volatile matter decreased to about 25% for 600-IROP.

The difference in fixed carbon and volatile matter contents between the hydrochars and biochars could be attributed to the used operating conditions, namely, (i) the carbonization media and (ii) the carbonization temperature. Indeed, the carbonization in presence of water induces the physico-chemical transformation of the media into a sub-critical fluid with significant presence of specified ionic entities [17]. The important moisture content reduces significantly the final mass loss and therefore the release of volatile matter. At extended reaction times, an important part of volatile matter ends up by being recombined and repolymerized in the structure of the sample [38]. The increase in heat intake by the material accelerates the degradation of the cellulose, hemicellulose, and then lignin along with volatile matter [26]. In fact, the increase in carbonization temperature is usually accompanied by the decrease in groups concentration such as methine (=CH–) and esters (–CO–OR), presenting the main components of the IROP aromatic structure. It has been reported that hydrothermal carbonization of raw olive pomace is generally governed by either dehydration or decarboxylation reactions yielding to the liberation of volatiles in the form of H_2O, CO and CO_2 [39]. When performing the pyrolysis at higher temperature,

the degradation of the lignocellulosic matrix intensifies towards the polymerization of the carbon content into a more stable aromatic structure. According to Chen et al. [40], the pyrolysis of various biomasses at temperatures varying between 300 °C and 600 °C is characterized by an increasing liberation of carbonic gases and methane with the increase of the temperature, suggesting the almost total degradation of their lignocellulosic structure.

The content in ash, as an indicator for minerals content in the feedstock and carbonaceous materials, slightly decreased from 11% to 5% for IROP and 180-IROP, respectively, then increased gradually until reaching 9% and 10% for 220-IROP and 600-IROP, respectively. The initial decrease of ash could be attributed to the elimination of some minerals at low carbonization temperatures especially potassium [41]. In the case of hydrochars, when increasing carbonization temperature, the volatile matter content reduced, and simultaneously, ash minerals content increased.

It is worth highlighting that unexpectedly for 600-IROP, the content in volatile matter slightly increased and fixed carbon decreased (Figure 1). The reason explaining this behavior is the thermal decomposition of oxygen-based functional groups (-COOH, -COOOR, CO, etc.) with the release of CO, CO_2 and H_2O species. The rest organic fragments such as phenols, lignin can lead also to the release other species such as CH_4, H_2 [42]. A similar outcome was reported by Jian et al. [43] when studying the production of biochars from rice husk under different temperatures. They showed that the fixed carbon contents increased from 39.7% to 47.4% for pyrolysis temperatures of 350 °C and 500 °C, respectively, then decreased to reach 46.6% for a pyrolysis temperature of 800 °C.

3.2. Ultimate and Elemental Analysis

The content in CHNS of the produced hydrochars and biochars were gathered in Table 1. The impregnated olive pomace shows a content in carbon and oxygen of ~ 45% and 44%, respectively. Such composition is roughly similar to the one found for abundant lignocellulosic materials such as rice husk [43], date palm seeds [44] or acacia wastes [45]. In comparison to non-impregnated olive pomace [26], the ROP impregnation by OMWW has led to a slight increase in C% and H% by 2.0% and 0.2%, respectively, and a decrease in O% by 2.5%. It has been reported that the addition of organic matter to the feedstock could enhance subsequently the final content in carbon [46].

Table 1. Ultimate analysis (db.%) of the IROP and its derived hydrochars and biochars at different carbonization temperatures.

	C (%)	H (%)	O (%)	N (%)	S (%)
IROP	44.76	5.83	44.04	1.97	0.18
180-IROP	57.34	5.80	34.94	0.70	0.10
200-IROP	61.73	5.89	28.68	0.99	0.16
220-IROP	66.15	6.11	23.75	1.45	0.09
400-IROP	92.47	2.12	1.84	0.94	0.08
500-IROP	90.90	1.08	2.47	0.75	0.12
600-IROP	90.33	0.6	3.18	0.40	0.13

The impact of hydrothermal carbonization on the ultimate composition of chars could be observed initially in the carbon content which increased from 45% to 66% for a carbonization temperature of 220 °C compared to the initial material (Table 1). On the contrary, for the same samples and temperature, the oxygen percentage decreased from 44% to 23% while hydrogen content remained globally constant. This behavior could be attributed to the effect of carbonization temperature on the degradation of cellulosic and hemicellulosic matrixes [47]. In fact, the in-depth heating of the organic biomasses generally leads to the defragmentation of the long chains of biopolymers into lower rank saccharides,

acids and alcohols and their migration towards the liquid phase, which explains the decrease in oxygen percentage in the hydrochars [48].

Similar behavior was noticed after the slow pyrolysis process where the biochars presented high contents of carbon (varying between 90 and 92%, (Table 1)). On the other hand, the content of hydrogen and oxygen noticeably dropped reaching values of 0.6% and 3.2%, respectively, for 600-IROP. Such outcome was expected as the increase of energetic uptake resulted in an acceleration in the feedstock's degradation process into a more stable carbonaceous material. It has been reported that the complete degradation of cellulose and hemicellulose structure occurs at 250 °C and 320 °C, respectively, with the liberation of volatile organic compounds (VOC) as well as CO and CO_2 gases [29,49]. For carbonization temperatures exceeding 350 °C, the degradation of lignin takes place with a higher release of VOC, which explains the decrease of (i) volatile matter content (Figure 1) and (ii) the decrease in hydrogen and oxygen contents [50,51].

To be more conclusive on the degradation mechanism path, a Van Krevelen diagram was elaborated on the basis of the ultimate analysis results. The O/C (degree of polarity) vs. H/C (degree of aromaticity) atomic ratios of raw, impregnated olive pomace and produced chars presented a rather uniform evolution tendency (Figure 2). The raw materials, i.e., raw and impregnated olive pomace, presented atomic ratios that are similar to widely used lignocellulosic feedstocks [17,52]. The impregnation of the ROP with the OMWW led to a slight decrease in O/C and H/C ratios compared to raw ROP, which confirms the successful transfer of organic matter from OMWW onto the feedstock. After increasing the carbonization temperature during HTC from 180 °C to 220 °C, the increase in carbon content led to a decrease in both O/C and H/C ratios from 0.45 to 0.26 and from 1.21 to 1.11, respectively. According to these ratios progress, the carbonization reaction could be driven mainly by a dehydration mechanism (Figure 2). It implies that the biomass transformation into a high-carbon-content material is associated with the liberation of protons from its surface and the generation of water and acidic entities into the carbonization media [26,53].

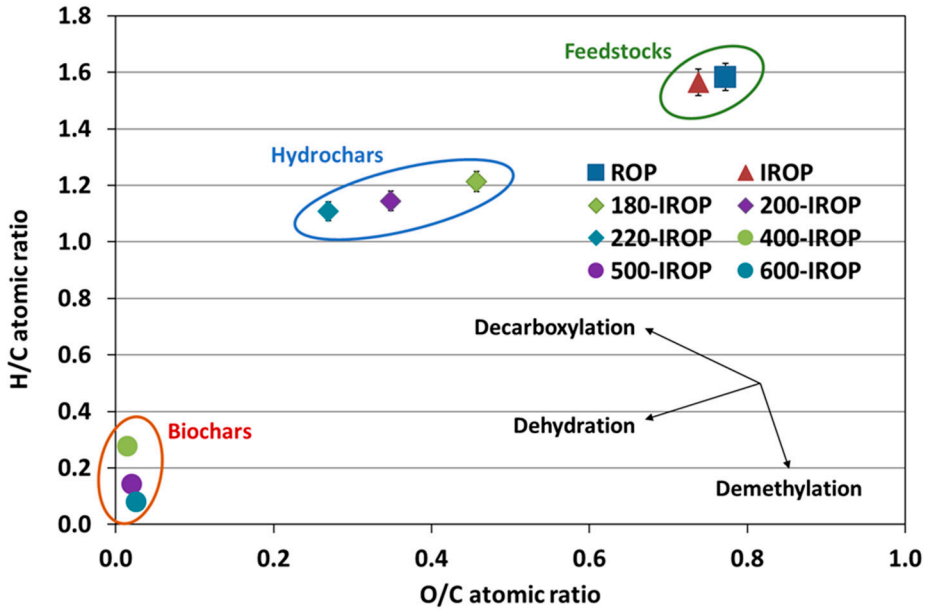

Figure 2. Van Krevelen diagram for IROP and its derived hydrochars and biochars produced at different temperatures.

Likewise, for the generated biochars, compared to the IROP, the atomic H/C and O/C ratios significantly decreased reaching values of only 0.02 and 0.08 for 600-IROP, respectively (Figure 2). These values suggest that IROP-derived biochars could be classified as higher-rank coals to anthracites materials characterized by important carbon and low impurities content with significant energetic added-value [17,54,55]. It can be remarked

nonetheless that the O/C ratio slightly decreased with increasing pyrolysis temperature. The OMWW is characterized by a significant content in organic compounds such as phenols and alcohols but most importantly organic acids such as D-Quinic, citric, succinic and methylmaleic acid [29,48]. The impregnation of such acidic entities onto ROP could lead to a dehydration process that results in an increase in carbon content but also in the release of water molecules [56]. However, when increasing the carbonization temperature, it seems that heat intake along with the presence of such molecules of high reactivity with organic biopolymers could result to the enhancement of VOC release [57]. Consequently, the impregnation of acid might result in a slight decrease in carbon content with an increase oxygen percentage and therefore a slight enhancement of its hydrophilicity.

The elemental composition of the IROP and produced hydrochars and biochars is presented in Table 2.

Table 2. Elemental composition (db.%) and HHV (MJ/kg) of IROP hydrochars and biochars produced at different temperatures.

	Potassium (g/kg)	Sodium (g/kg)	Calcium (g/kg)	Magnesium (g/kg)	Phosphorus (g/kg)	Sum of Minerals (g/kg)	HHV (MJ/kg)
IROP	5.40	0.52	0.87	0.14	0.17	7.11	18.48
180-IROP	0.75	0.07	0.82	0.05	0.01	1.71	19.40
200-IROP	0.80	0.11	0.91	0.06	0.01	1.89	22.55
220-IROP	1.15	0.13	0.99	0.12	0.01	2.42	28.75
400-IROP	2.74	0.32	1.10	0.25	0.12	4.53	25.74
500-IROP	3.08	0.50	1.21	0.31	0.14	5.24	27.19
600-IROP	3.10	0.39	1.39	0.30	0.16	5.34	29.78

After hydrothermal carbonization, the content in minerals globally decreased for all samples. For instance, the content in potassium, magnesium and phosphorus decreased by about 86%, 66% and 92% after a carbonization at 180 °C, respectively (Table 2). However, the increase in carbonization temperature seems to constantly enhance their concentrations in hydrochars. In fact, the sum of minerals increased by 42% when increasing the treatment temperature from 180 °C to 220 °C, respectively. This behavior is attributed to the simultaneous effect of increasing carbonization temperature and reaction time. While an increase in inner heat tends to stimulate the leaching of minerals in the liquid fraction, extended reaction times increase the contact time between the liquid media charged with minerals and organic and the hydrochar. The HTC was widely used as a method for pretreatment of precursors before the thermal activation in order to produce high-quality carbonaceous materials with low impurities [58]. This step usually aims to induce some specific modifications on the surface characteristics but also to catalyze the release of impurities from the char. The cumulative effect of pressure, water vapor and heat diffusion could generate antagonist reactions, leading to the degradation of the lignocellulosic and lipids contents into soluble molecules then their recombination and repolymerization onto a hydrophilic hydrochar surface [26]. The reintegration of these organic compounds could be accompanied eventually with the "re-adsorption" of the released minerals. Similar outcome was reported by Volpe et al. [59] when studying the hydrothermal carbonization of Opuntia ficus-indica at different temperatures. The authors suggested that the increase in carbonization degree enhances a possible interaction between the minerals and the released gases during the process which weakens their depletion from the organic structure.

Compared to hydrochars, the pyrolysis of IROP led to biochars with significantly high contents in minerals. In fact, the sums of minerals contents were 4.53 and 5.34 g/kg for treatment temperatures varying between 400 °C and 600 °C, respectively (Table 2). These increases are related to the effect of temperature on the chemical and structural properties of the final material. The increase in the treatment temperature led to a reduction

of volatile matter and the stabilization of the aromatic structure into a higher carbon-content biochar. The decrease in volatile matter allowed the immobilization of minerals either by diffusion in the pores (Van der Waals or hydrogen bonds) or anchored inside the structure by electrostatic bonds in the form of crystals [50]. Similar results were reported by Zhao et al. [60] when studying the effect of pyrolysis temperature variation on final biochars mineral properties. The authors suggested an increase in mineral content of potassium (+96%), calcium (+96%), magnesium (+97%) and phosphorus (+95%) for wheat straw pyrolysis performed between 350 and 650 °C.

3.3. Energetic Properties

The energetic properties of the biochars and hydrochars are presented in Table 2. It can be seen that the calorific potential of the impregnated olive pomace (18.48 MJ/kg) was higher than various used feedstocks such as rice husk (17.23 MJ/kg; Vieira et al. [61]) and microalgae (11.10 MJ/kg; Teh et al. [62]).

The hydrothermal carbonization led to an enhancement of the calorific properties of the resulting hydrochars. Indeed, the corresponding HHV values vary between 19.40 and 28.75 MJ/kg for experiments performed at 180 °C and 220 °C, respectively. Similar trend was remarked for the produced biochars were the HHV values reach 25.74 and 29.78 MJ/kg for pyrolysis temperatures ranging between 400 °C and 600 °C, respectively. The addition of OMWW to the raw feedstock enhanced considerably the recorded heating values. For instance, by comparing the current results to our previous study where the HTC of ROP was performed in water, the HHV increased by only 19% for a carbonization temperature of 220 °C [26]. The increase of the carbonization temperature through a dry process, i.e., slow pyrolysis, promoted the liberation of volatile matter with low calorific value such as cellulose, hemicellulose and phenols [63]. The decrease in oxygen and hydrogen content led to the acceleration of a cross-linking reaction with the lignin aromatic structure, yielding a more stable carbonaceous biochar characterized by interesting calorific potential.

3.4. Morphological Properties

Microscopic imagery for the raw and carbonized materials are presented in the Figure 3. The impregnated olive pomace presents a rough and heterogeneous surface with small cavities related to the lignocellulosic matrix endings and similar to the majority of biomass structures [26,64]. By applying different carbonization techniques, the recovered materials show very dissimilar aspects (Figure 3). Indeed, the surface of hydrochars exhibits interconnected sphere-like particles with different diameters. The formation of these structures is attributed to the degradation mechanism of cellulosic structure into small chained polymers such as hydroxymethylfurfural (5-HMF) and furfural through dehydration reaction [26,65]. For extended carbonization time, these short aldehydes were repolymerized on the surface of the carbon material leading to spherical carbon condensates with hydrophilic outer shell (high content in oxygen groups) and a hydrophobic porous core [66]. According to the images, the hydrochars spheres produced at 180 °C seem to be incompletely developed compared to the one observed for 220-IROP. At a carbonization temperature of 200 °C and 220 °C, these spherical particles became easily identified with a significant and homogeneous concentration, by presenting chain-like aggregations. Unlike the observations found in literature related to the carbonization of xylose, where the resulting spheres are isolated and with fairly monotonous diameters [67], carbonization of both IROP led to the formation of interconnected and relatively voluminous spheres (>0.3 μm) related to the fructose-based carbons.

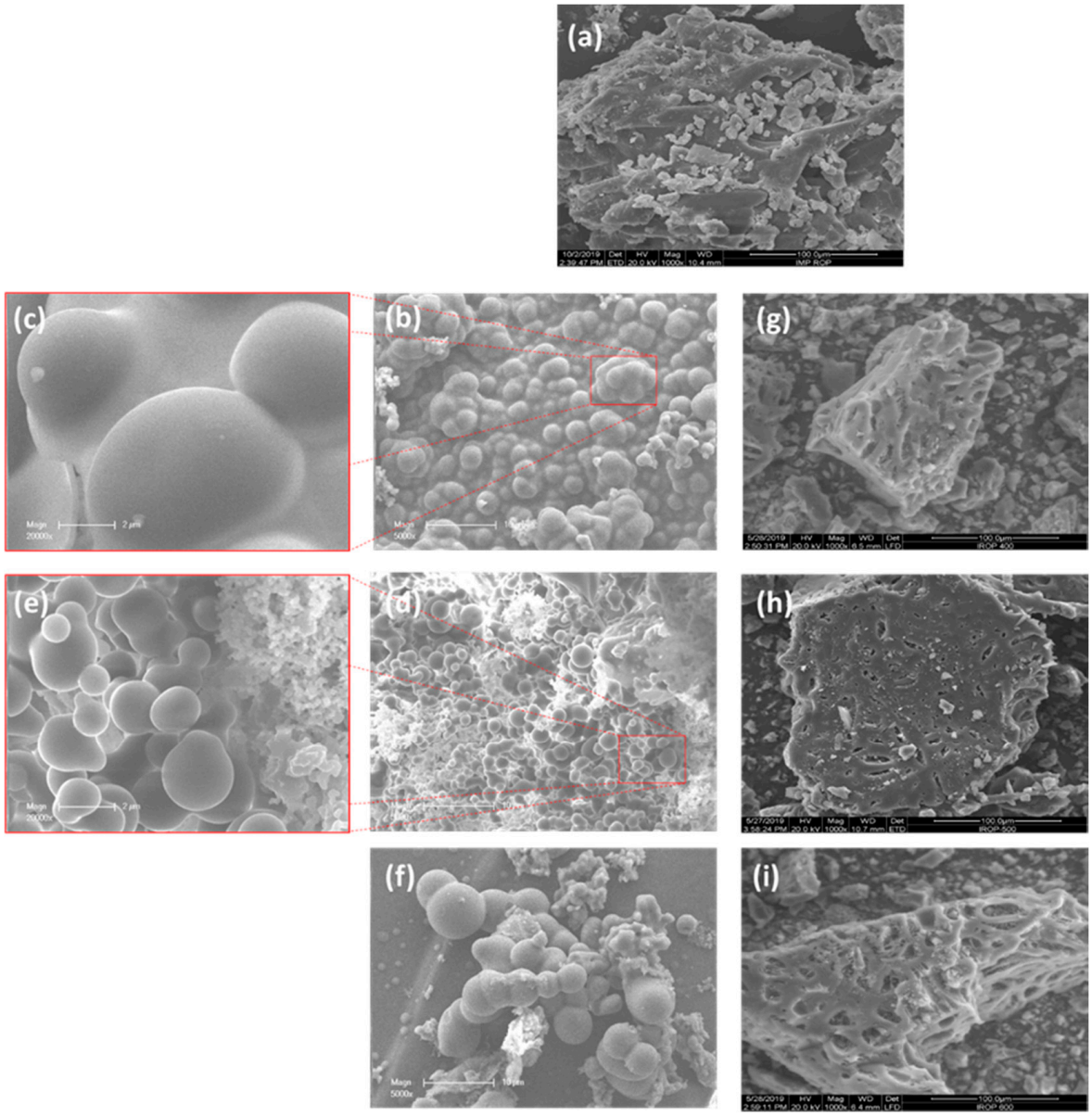

Figure 3. Scanning electron microscope images of (**a**) impregnated raw olive pomace and the produced (**b**–**f**) hydrochars and (**g**–**i**) biochars under different carbonization conditions.

The slow pyrolysis seems to bring more intense modifications on the materials, leading to formation of biochars with rough and more sharp-edged particles compared to hydrochars (Figure 3g–i). Moreover, the chars show a more developed porosity compared to hydrochar. This suggests a possible in-depth heat transfer towards the core of the materials with increasing carbonization temperature. The early degradation of cellulose and hemicellulose at a temperature range between 200 °C and 230 °C in the form of volatile matter increased the concentration of carbon content and therefore enhanced the aromatic porous skeleton of lignin matrix [68].

To apprehend the main structural differences between hydrochars and biochars produced from IROP, XRD analysis was conducted, and results were gathered in Figure 4. The main differences were spotted in the diffraction angles between 10° and 50° (2θ). The IROP presented a typical diffractogram to the majority of biomasses, characterized by amorphous cellulose I double peaks at 14.8° and 22.5° (2θ) [64]. After HTC, the resulting materials produced at 180 and 200 °C presented almost similar aspects. In fact, the peaks related to cellulose I kept the same position, but they increased in intensity and developed a more

defined form. This behavior indicates the beginning of a possible degradation reaction of cellulose I into a more stable carbon form. When increasing the treatment temperature (220 °C), the cellulose peaks disappeared into a broad peak at 22.6° (2θ) which indicates its transformation into a disordered-like carbon [69]. On the other hand, raw and HTC produced materials presented a significant content in minerals, namely, SiO_2, $CaCO_3$ and Fe_2O_3. The presence of these impurities is associated with the natural composition of the biomass as well as the stocking conditions of the used impregnated feedstock [29].

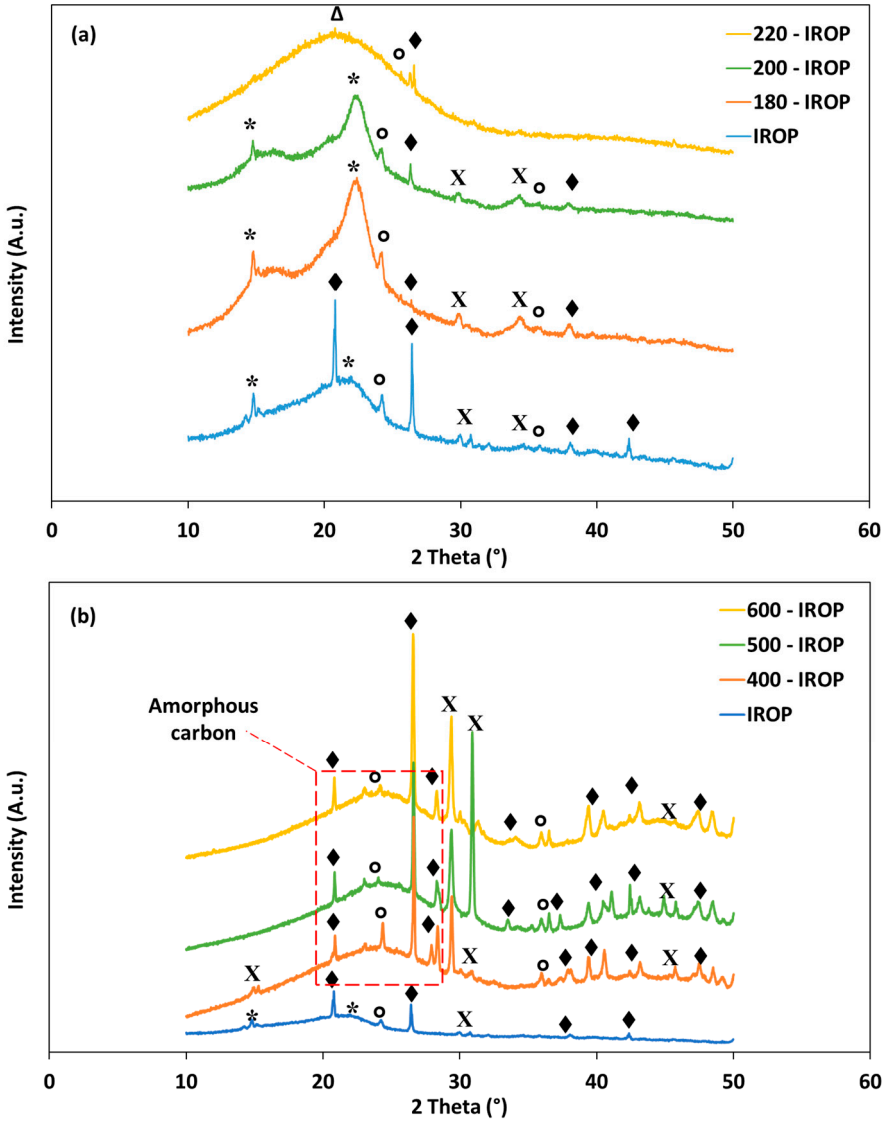

Figure 4. X-ray diffractograms for IROP and the resulting (**a**) hydrochars and (**b**) biochars produced at 180, 200, 220 °C and 400, 500 and 600 °C, respectively (*: Cellulose I, Δ: Amorphous cellulose, ♦: SiO_2, X: $CaCO_3$, ○: Fe_2O_3).

It can be remarked nonetheless that the content in minerals significantly decreased at higher HTC temperature (Figure 4a). The majority of peaks attributed to calcium carbonate and quartz disappeared at 220 °C alongside the significant transformations in the aromatic lignocellulosic structure. The increase in carbonization temperature and the effect of water ionization into more stable radicals enhanced the degradation of the material and thereby the production of multiple acidic forms further promoting the cleavage of the surface of the material [69]. It has been reported that such outcome driven by a dehydration reaction leads generally to a decrease in oxygenic surface groups and eventually the leaching of min-

erals [70,71]. However, it is also possible that the decrease in peaks intensity is correlated to the amorphization of the crystalline forms due to the increase in HTC temperature.

The slow pyrolysis exhibited a very different structure with an enhanced crystallinity of the minerals (Figure 4b). In fact, the peaks related to calcium carbonate and quartz were significantly present in diffraction angles varying between 30° and 50° (2θ). It is possible that the increase in pyrolysis temperature has enhanced the fixation of minerals with a more arranged form into stable carbon structure [72]. Similar findings were reported by Igalavithana et al. [73] when producing biochars from food waste for CO_2 adsorption from gaseous phase. XRD analysis emphasized the increase in mineral crystallization when increasing pyrolysis temperature, especially for calcite, whewellite and halite (NaCl). Moreover, the pyrolysis seems to promote the modification of the aromatic structure of the biomass into a more carbon-content material. In fact, a shift in the Cellulose I peaks was noted from 22.4° to a broad pic varying between 20° and 30° (2θ) describing the (002) spacing between the formed carbon interlayers [74].

3.5. Surface Chemical Properties

Infrared spectroscopy was performed on hydrochars and biochars produced from IROP and results were gathered in Figure 5. The recovered spectra show the presence of five main peak areas, namely –OH, C=O, C=C, $–CH_2/CH_3$, C–O and aromatic –CH, which exhibit a significant profile change with the applied conditions.

The impregnated raw olive pomace presented a typical profile of lignocellulosic materials, characterized by a large hydroxyl band between 3800 and 3200 cm^{-1}, aliphatic stretch bands between 2920 and 2870 cm^{-1}, vibrations related to hemicellulose structure at 1720 cm^{-1} and finally the polar C–O stretch related to vibrations of cellulose and lignin located at about 1100 cm^{-1} [29,75].

After hydrothermal carbonization, the peaks corresponding to –OH groups decreased in intensity when increasing the temperature at the exception of the hydrochar produced at 200 °C. According to Sevilla and Fuertes [76], this behavior could be linked to a possible dehydration reaction. The slight increase in the intensity of hydroxyl band for 200-IROP might be caused by the recombination of saccharides and polyphenols on the surface of the hydrochar. In fact, the degradation of holocellulose into small-chained biopolymers is not complete at this temperature, and the recombination of the degradation by-products on the surface of hydrochars is possible which is in concordance with the SEM images (see Figure 3). Furthermore, an increase in the peak wavenumber of the C=O band from -21 cm^{-1} to -56 cm^{-1} was detected when increasing carbonization temperature between 180 °C and 220 °C (Figure 5a). A similar behavior was noticed for the aromatic C=C bonds where the related peak shifted by -19 cm^{-1} to -47 cm^{-1} for the same HTC temperatures (Figure 5a). This could be attributed to a stretch in the aromatic skeletal of the lignin matrix [26]. Some deformations could be also remarked as -CH_2/CH_3 and carbonyl C-O aromatic bends shifted by +12 cm^{-1} and +25 cm^{-1} for IROP and 220-IROP, respectively.

On the other hand, for the pyrolyzed samples, the broad hydroxyl peak between 3800 cm^{-1} and 3200 cm^{-1} has disappeared even at relatively low pyrolysis temperatures (Figure 5b). Similar observation is valid for the C=O ester groups, where corresponding peak found for the feedstock at 1720 cm^{-1} disappeared at 400 °C. Moreover, the carbonyl (–C–O) peak detected at 1100 cm^{-1} decreased in intensity until disappearing at a pyrolysis temperature of 600 °C. This could be attributed to the slow degradation of cellulose and hemicellulose. On the other hand, the peaks corresponding to aromatic groups, notably the aliphatic =C–H at 2870 cm^{-1}, C–H carbohydrates and lignin deformation group at 1650 cm^{-1} and aromatic band at 876 cm^{-1} remained unchanged even at higher pyrolysis temperature. According to Zhang et al. [77], in case of an initial abundance of functionalities, this behavior could be attributed to the pyrolysis mechanism for the condensation of carbon in the solid fraction and the release of oxygen in the form of CO_2 gas [42,78], suggesting the maintenance of the aromatic skeleton of the lignin structure at pyrolysis temperatures

varying between 400 and 600 °C. Therefore, it appears that the biochar materials have significantly poorer surface chemistry than hydrochars.

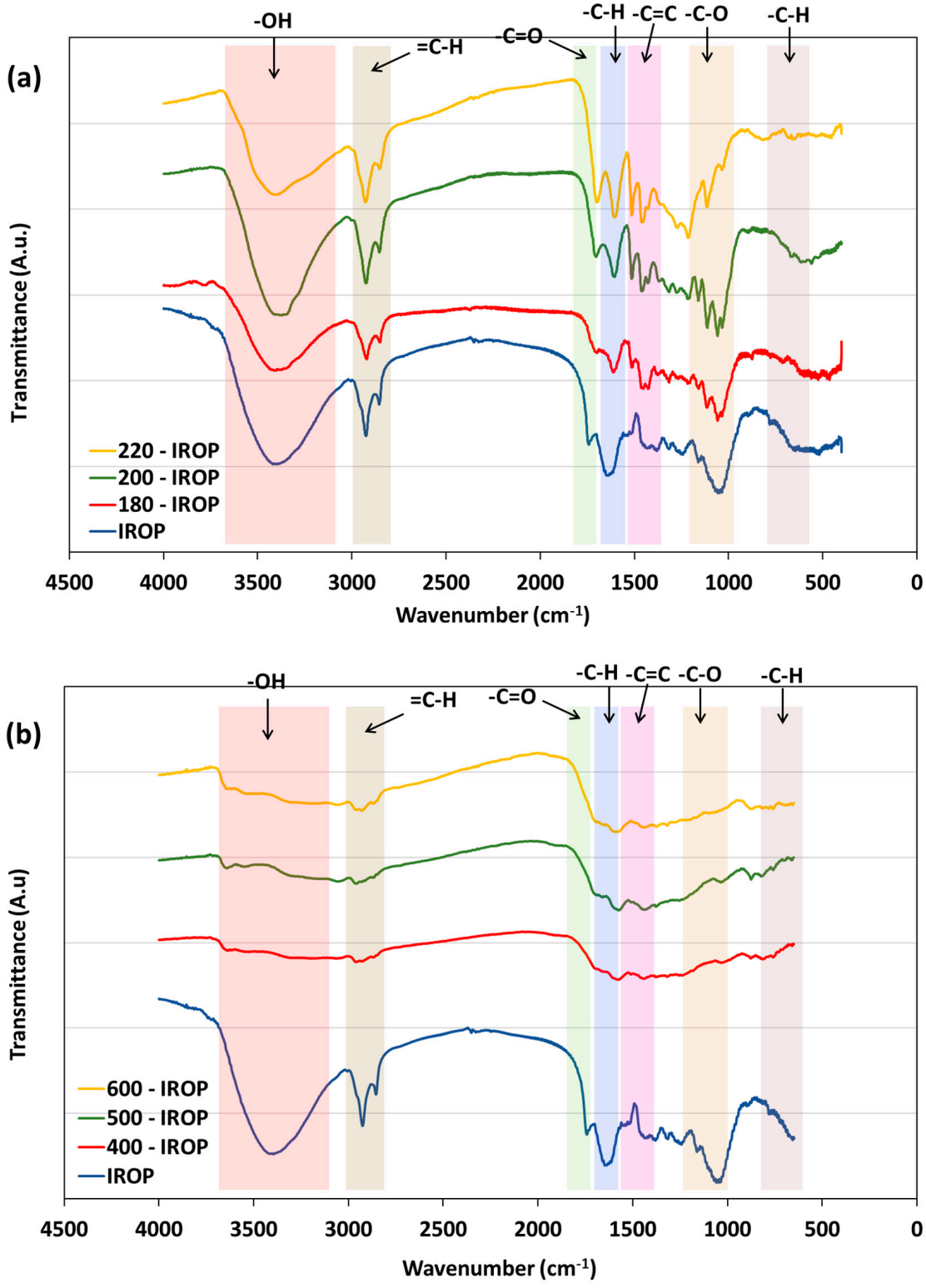

Figure 5. Fourier transform infrared spectroscopy for IROP and the resulting (**a**) hydrochars and (**b**) biochars produced at 180, 200, 220 °C and 400, 500 and 600 °C, respectively.

To have a conclusive idea about the nature and the quantity of the chars' surface functional groups, the functional groups via Boehm titration and pH_{zpc} were assessed, and results were gathered in Table 3.

Table 3. Acidic and basic functional groups concentrations (µmol/g), final solution pH and surface pH at zero-point charge (pH_{zpc}) of the impregnated raw olive pomace and the produced hydrochars and biochars from the HTC and slow pyrolysis at 180, 200, and 220 and at 400, 500, and 600 °C, respectively (–: unmeasurable property; U.D.: undetected measurement).

	Functional Groups (µmol/g)					Final Solution pH	pH_{zpc}
Sample	**Carboxylic**	**Lactonic**	**Phenolic**	**Basic**	**Total**		
IROP	611.62	35.47	638.48	1347.85	2633.42	–	5.24
180-IROP	360.89	9.44	493.62	U.D.	863.95	3.96	4.16
200-IROP	457.48	74.68	555.96	U.D.	1088.12	4.13	3.84
220-IROP	523.05	294	438.01	U.D.	1255.06	4.08	3.28
400-IROP	65.22	24.22	71.94	76.10	237.48	–	8.47
500-IROP	26.84	8.45	99.41	134.74	269.44	–	9.15
600-IROP	12.45	U.D.	126.18	158.15	296.78	–	9.51

The heterogeneous aspect of the impregnated pomace could be noticed by the presence of both acidic (total quantity = 1285.57 µmol/g) and basic groups (1347.85 µmol/g). These results are in agreement with those reported by previous studies handling lignocellulosic materials [32,79]. These values were highly affected by the type of thermal conversion as well as the increase in treatment temperature (Table 3). Indeed, in the case of hydrothermal carbonization, a significant decrease in acidic functional was noted even at low temperatures. For instance, compared to the IROP, the content in carboxylic, lactonic and phenolic functions decreased by about 41%, 73% and 23%, respectively, when performing HTC at 180 °C (Table 3). This tendency is related to the degradation mechanism of the biomass leading to the dissociation of acids under the effect of temperature and the elimination of volatile matter. However, the total acidic groups content increased by 45% when rising the temperature from 180 to 220 °C. It has been reported by Saha et al. (2019) [79] that the HTC of wood at temperatures varying between 180 and 260 °C led to an enhancement in lactonic and carboxylic groups content. The hydrolysis mechanism favored the simultaneous degradation mechanism of different matrices of the biomass towards the recombination of these acids at higher severity conditions. On the other hand, the basic functional groups were not detected for all hydrochars. Despite their confirmed presence using FTIR analysis technique, the detection of basic groups was limited by the Boehm method. This could be due to the possible saturation of the titration solution with the soluble acidic groups of the hydrochar which compromised the analysis procedure.

Concerning the generated biochars, it appears that the pyrolysis process induces an important decrease in the total functional groups' contents. For instance, compared to the IROP, a decrease of about 91% was observed for 400-IROP. According to the results presented in Table 3, the total contents of acidic and basic groups were significantly low compared to the raw feedstock and the hydrochars which could be explained by the effect of heat uptake and the scouring under high temperature treatment. Moreover, with the increase of the pyrolysis temperature, the total content of acidic functional groups diminished whereas the content of basic functional groups increased. The reasons behind this behavior will be explained in the following paragraph.

These findings were further confirmed when performing pH ZPC analysis (Table 3). The impregnation of ROP by olive mill wastewater increased the surface acidity of the biomass, with a decrease in the pH_{zpc} from 5.84 to 5.24 for ROP and IROP, respectively [26]. This outcome was predictable since the OMWW contains significant concentrations of

organic acids [29,48]. After HTC, the pH_{zpc} values decreased significantly by increasing the temperature, i.e., 4.16 to 3.28 for 180-IROP and 220-IROP, respectively (Table 3). The increase in HTC temperature was proven to yield higher concentrations of soluble acids in the liquid media during the degradation of the holocellulose matrix. The increasing severity conditions, i.e., rise in heat intake, leads to higher water vapor pressure causing a scouring of the biomass surface, the depolymerization of the cellulose into soluble acids and eventually their recombination on the surface of the hydrochars [29]. This mechanism is further confirmed by the pH of recovered water after carbonization, i.e., 4.08 for 220-IROP which decreased compared to that of deionized water (pH = 6.5) (Table 3). It was reported in our previous work that acids such as dicarboxylic, monosaccharide and other small organic acids that contributed to the decrease of pH values were proven to be beneficial in the case of agricultural applications as a liquid soil amendment [26].

For the biochars, it appears that the pyrolysis of IROP under inert atmosphere led to a significant increase in the surface pH (Table 3). In fact, the pH_{zpc} increased from 8.47 to 9.51 when increasing pyrolysis temperature from 400 to 600 °C, respectively. Based on the previously performed analysis, slow pyrolysis enhances the alkalinity of the biochars surface according to the following two simultaneous chemical pathways: (i) the heat uptake on the lignocellulosic material leads not only the alteration of the aromatic structure towards the fixation of carbon but also the elimination of volatile matter, notably polyphenols and volatile organic acids. Consequently, oxygen–based groups concentrations decrease significantly with increasing carbonization temperature, thus yielding a surface with less acidic groups; (ii) the rearrangement of the aromatic structure into more fixed carbon content and even towards graphite-structure goes along with the immobilization of alkaline and alkaline earth metals (Ca^{2+}, Mg^{2+}, K^{+}, Na^{+}, etc.) in crystalline forms [42,72,80]. The presence of these ions, even at low concentrations, leads to more alkaline biochar surface. It is important to underline that the type of the functional groups (acidic or basic) significantly impacts the effectiveness of solid materials in removing both organic and mineral pollutants from aqueous solutions [18].

4. Conclusions

In this research work, hydrochars and biochars from raw olive pomace impregnated with olive mill wastewaters were synthesized under different experimental conditions and then characterized in depth. Results showed that the final products presented significantly different physico-chemical properties that are intimately related to the used treatment process. Indeed, hydrothermal carbonization led to hydrochars with higher volatile matter and low carbon contents compared to biochars. Moreover, nutrients contents (such as magnesium, potassium and sodium) were significantly high for biochars due to the immobilization phenomenon at high treatment temperatures. Moreover, the carbonization in presence of water promoted the depolymerization of the biomass, through the dehydration mechanism, into large number of long/short chained acids and saccharides. The extended HTC time caused a repolymerization of these organic compounds on the surface of the hydrochar in a specific fashion in the form of sphere-like carbons. These structures were rather absent in the case of biochars, where the surface is roughly heterogeneous characterized by the presence of pores in the form of slits. The pyrolysis of IROP under inert atmosphere at relatively high temperatures (up to 600 °C) led to an important elimination of oxygen which resulted in a net decrease of O/C and H/C ratios as well as a significant reduction of surface functional groups concentrations with an alkaline-dominated surface. On the other hand, moderate hydrothermal carbonization gives hydrochars with acidic pH_{zpc} due to the high contents of carboxylic, phenolic and lactonic groups. These results indicated that the produced hydrochars could be used in agriculture as a biofertilizer and also for the removal of cationic pollutants (i.e., ammonium) from aqueous solutions. These generated biochars could be effective in removing anionic contaminants such orthophosphates. To give a new life to these produced hydrochars and biochars for sustainable agriculture and

environment preservation, further experimental work at laboratory (static and dynamic conditions) and field scales has to be undertaken.

Author Contributions: Conceptualization, C.M.G. and M.J.; methodology, A.A.A., C.M.G. and M.J.; validation, C.M.G., S.J. and M.J.; formal analysis, A.A.A., C.M.G. and M.J.; investigation, A.A.A. resources, L.E.-B.; data curation, A.A.A. and L.E.-B.; writing—original draft preparation, A.A.A.; writing—review and editing C.M.G., S.J. and M.J.; supervision, C.M.G., S.J. and M.J.; project administration, C.M.G. and M.J.; funding acquisition, C.M.G., M.J. and S.J. All authors have read and agreed to the published version of the manuscript.

Funding: This work was funded by FERTICHAR project—European Union's Seventh Framework Program for research, technological development and demonstration (ANR-17-ARM2-0009 through ERA-NET ARIMNet2 call) under grant agreement No. 618127.

Institutional Review Board Statement: Not applicable.

Informed Consent Statement: Not Applicable.

Data Availability Statement: Not Applicable.

Acknowledgments: The authors gratefully acknowledge the funding agencies for their support. The authors also wish to thank all the personnel operating the technical platforms of the IS2M for their scientific contributions and their help for the careful running of the experiments and analyzes.

Conflicts of Interest: The authors declare no conflict of interest.

References

1. Reardon, T.; Barrett, C.B.; Berdegué, J.A.; Swinnen, J.F.M. Agrifood Industry Transformation and Small Farmers in Developing Countries. *World Dev.* **2009**, *37*, 1717–1727. [CrossRef]
2. Kerr, W.A. Agriculture after a year with COVID-19: Any long-term implications for international trade policy? *Can. J. Agric. Econ. Can. D'Agroecon.* **2021**, *69*, 261–267. [CrossRef]
3. Rochman, G.P.; Indratno, I.; Agustina, I.H. Rural Agri-Food Industry Resilience in Indonesia. *IOP Conf. Ser. Earth Environ. Sci.* **2021**, *830*, 012063. [CrossRef]
4. Laura, L.; Osorio, D.R.; Flórez-López, E.; David Grande-Tovar, C.; Flórez-López, E.; Grande-Tovar, C.D.; Trombetta, D. The Potential of Selected Agri-Food Loss and Waste to Contribute to a Circular Economy: Applications in the Food, Cosmetic and Pharmaceutical Industries. *Molecules* **2021**, *26*, 515.
5. Hadroug, S.; Jellali, S.; Jeguirim, M.; Kwapinska, M.; Hamdi, H.; Leahy, J.J.; Kwapinski, W. Static and dynamic investigations on leaching/retention of nutrients from raw poultry manure biochars and amended agricultural soil. *Sustainability* **2021**, *13*, 1212. [CrossRef]
6. Vandeponseele, A.; Draye, M.; Piot, C.; Chatel, G. Subcritical water and supercritical carbon dioxide: Efficient and selective eco-compatible solvents for coffee and coffee by-products valorization. *Green Chem.* **2020**, *22*, 8544–8571. [CrossRef]
7. Hadj Saadoun, J.; Bertani, G.; Levante, A.; Vezzosi, F.; Ricci, A.; Bernini, V.; Lazzi, C. Fermentation of Agri-Food Waste: A Promising Route for the Production of Aroma Compounds. *Foods* **2021**, *10*, 707. [CrossRef]
8. Wahab, M.A.; Hassine, R.B.; Jellali, S. *Posidonia oceanica* (L.) fibers as a potential low-cost adsorbent for the removal and recovery of orthophosphate. *J. Hazard. Mater.* **2011**, *191*, 333–341. [CrossRef]
9. Hadroug, S.; Jellali, S.; Leahy, J.J.; Kwapinska, M.; Jeguirim, M.; Hamdi, H.; Kwapinski, W. Pyrolysis process as a sustainable management option of poultry manure: Characterization of the derived biochars and assessment of their nutrient release capacities. *Water* **2019**, *11*, 2271. [CrossRef]
10. Bolaji, I.; Nejad, B.; Billham, M.; Mehta, N.; Smyth, B.; Cunningham, E. Multi-criteria decision analysis of agri-food waste as a feedstock for biopolymer production. *Resour. Conserv. Recycl.* **2021**, *172*, 105671. [CrossRef]
11. Abdeshahian, P.; Ascencio, J.J.; Philippini, R.R.; Antunes, F.A.F.; de Carvalho, A.S.; Abdeshahian, M.; dos Santos, J.C.; da Silva, S.S. Valorization of Lignocellulosic Biomass and Agri-food Processing Wastes for Production of Glucan Polymer. *Waste Biomass Valoriz.* **2020**, *12*, 2915–2931. [CrossRef]
12. Beda, A.; Le Meins, J.M.; Taberna, P.L.; Simon, P.; Matei Ghimbeu, C. Impact of biomass inorganic impurities on hard carbon properties and performance in Na-ion batteries. *Sustain. Mater. Technol.* **2020**, *26*, e00227. [CrossRef]
13. Ciszewski, M.; Koszorek, A.; Radko, T.; Szatkowski, P.; Janas, D. Review of the Selected Carbon-Based Materials for Symmetric Supercapacitor Application. *J. Electron. Mater.* **2018**, *48*, 717–744. [CrossRef]
14. Landin-Sandoval, V.J.; Mendoza-Castillo, D.I.; Bonilla-Petriciolet, A.; Aguayo-Villarreal, I.A.; Reynel-Avila, H.E.; Gonzalez-Ponce, H.A. Valorization of agri-food industry wastes to prepare adsorbents for heavy metal removal from water. *J. Environ. Chem. Eng.* **2020**, *8*, 104067. [CrossRef]

15. Fernández-López, J.A.; Miñarro, M.D.; Angosto, J.M.; Fernández-Lledó, J.; Obón, J.M. Adsorptive and Surface Characterization of Mediterranean Agrifood Processing Wastes: Prospection for Pesticide Removal. *Agronomy* **2021**, *11*, 561. [CrossRef]
16. Hadroug, S.; Jellali, S.; Amine, A.; Marzena, A.; Helmi, K.; James, H. Valorization of salt post-modified poultry manure biochars for phosphorus recovery from aqueous solutions: Investigations on adsorption properties and involved mechanism. *Biomass Convers. Biorefin.* **2021**. [CrossRef]
17. Azzaz, A.A.; Khiari, B.; Jellali, S.; Ghimbeu, C.M.; Jeguirim, M. Hydrochars production, characterization and application for wastewater treatment: A review. *Renew. Sustain. Energy Rev.* **2020**, *127*, 109882. [CrossRef]
18. Jellali, S.; Khiari, B.; Usman, M.; Hamdi, H.; Charabi, Y.; Jeguirim, M. Sludge-derived biochars: A review on the influence of synthesis conditions on pollutants removal efficiency from wastewaters. *Renew. Sustain. Energy Rev.* **2021**, *144*, 111068. [CrossRef]
19. Jellali, S.; Charabi, Y.; Usman, M.; Al-Badi, A.; Jeguirim, M. Investigations on biogas recovery from anaerobic digestion of raw sludge and its mixture with agri-food wastes: Application to the largest industrial estate in Oman. *Sustainability* **2021**, *13*, 3698. [CrossRef]
20. Dutournié, P.; Jeguirim, M.; Khiari, B.; Goddard, M.-L.; Jellali, S. Olive Mill Wastewater: From a Pollutant to Green Fuels, Agricultural Water Source, and Bio-Fertilizer. Part 2: Water Recovery. *Water* **2019**, *11*, 768. [CrossRef]
21. Fan, H.; Gu, J.; Hu, S.; Yuan, H.; Chen, Y. Co-pyrolysis and co-gasification of biomass and polyethylene: Thermal behaviors, volatile products and characteristics of their residues. *J. Energy Inst.* **2019**, *92*, 1926–1935. [CrossRef]
22. Lu, J.S.; Chang, Y.; Poon, C.S.; Lee, D.J. Slow pyrolysis of municipal solid waste (MSW): A review. *Bioresour. Technol.* **2020**, *312*, 123615. [CrossRef] [PubMed]
23. Heidarinejad, Z.; Dehghani, M.H.; Heidari, M.; Javedan, G.; Ali, I.; Sillanpää, M. Methods for preparation and activation of activated carbon: A review. *Environ. Chem. Lett.* **2020**, *18*, 393–415. [CrossRef]
24. Savou, V.; Grause, G.; Kumagai, S.; Saito, Y.; Kameda, T.; Yoshioka, T. Pyrolysis of sugarcane bagasse pretreated with sulfuric acid. *J. Energy Inst.* **2019**, *92*, 1149–1157. [CrossRef]
25. Wang, T.; Zhai, Y.; Zhu, Y.; Li, C.; Zeng, G. A review of the hydrothermal carbonization of biomass waste for hydrochar formation: Process conditions, fundamentals, and physicochemical properties. *Renew. Sustain. Energy Rev.* **2018**, *90*, 223–247. [CrossRef]
26. Azzaz, A.A.; Jeguirim, M.; Marks, E.A.N.; Rad, C.; Jellali, S.; Goddard, M.-L.; Ghimbeu, C.M. Physico-chemical properties of hydrochars produced from raw olive pomace using olive mill wastewater as moisture source. *Comptes Rendus. Chim.* **2021**, *23*, 635–652. [CrossRef]
27. Marks, E.A.N.; Kinigopoulou, V.; Akrout, H.; Azzaz, A.A.; Doulgeris, C.; Jellali, S.; Rad, C.; Sánchez Zulueta, P.; Tziritis, E.; El-Bassi, L.; et al. Potential for Production of Biochar-Based Fertilizers from Olive Mill Waste in Mediterranean Basin Countries: An Initial Assessment for Spain, Tunisia, and Greece. *Sustainability* **2020**, *12*, 6081. [CrossRef]
28. Haddad, K.; Jeguirim, M.; Jerbi, B.; Chouchene, A.; Dutournié, P.; Thevenin, N.; Ruidavets, L.; Jellali, S.; Limousy, L. Olive Mill Wastewater: From a Pollutant to Green Fuels, Agricultural Water Source and Biofertilizer. *ACS Sustain. Chem. Eng.* **2017**, *5*, 8988–8996. [CrossRef]
29. Azzaz, A.A.; Jeguirim, M.; Kinigopoulou, V.; Doulgeris, C.; Goddard, M.-L.; Jellali, S.; Matei Ghimbeu, C. Olive mill wastewater: From a pollutant to green fuels, agricultural and water source and bio-fertilizer—Hydrothermal carbonization. *Sci. Total Environ.* **2020**, *733*, 139314. [CrossRef]
30. Bargaoui, M.; Jellali, S.; Azzaz, A.A.; Jeguirim, M.; Akrout, H. Optimization of hybrid treatment of olive mill wastewaters through impregnation onto raw cypress sawdust and electrocoagulation. *Environ. Sci. Pollut. Res.* **2020**, *28*, 24470–24485. [CrossRef]
31. Thompson, W.; Leege, P. Test methods for the examination of composting and compost. *Commun. Soil Sci. Plant Anal.* **1998**.
32. Azzaz, A.A.; Jellali, S.; Akrout, H.; Assadi, A.A.; Bousselmi, L. Optimization of a cationic dye removal by a chemically modified agriculture by-product using response surface methodology: Biomasses characterization and adsorption properties. *Environ. Sci. Pollut. Res.* **2016**, *11*, 9831–9846. [CrossRef]
33. DIN. *Testing of Solid and Liquid Fuels: Determination of Gross Calorific Value by the Bomb Calorimeter and Calculation of Net Calorific Value—Part 3: Method Using Adiabatic Jacket*; Deutsches Institut für Normung (DIN): Berlin, Germany, 2005; pp. 51900–51903.
34. Olszewski, M.P.; Nicolae, S.A.; Arauzo, P.J.; Titirici, M.M.; Kruse, A. Wet and dry? Influence of hydrothermal carbonization on the pyrolysis of spent grains. *J. Clean. Prod.* **2020**, *260*, 121101. [CrossRef]
35. Arauzo, P.J.; Maziarka, P.A.; Schoder, K.A.; Pfersich, J.; Ronsse, F.; Kruse, A. Influence of sequential HTC pre-treatment and pyrolysis on wet food-industry wastes: Optimisation toward nitrogen-rich hierarchical carbonaceous materials intended for use in energy storage solutions. *Sci. Total Environ.* **2021**, 151648. [CrossRef]
36. Sun, Y.; Gao, B.; Yao, Y.; Fang, J.; Zhang, M.; Zhou, Y.; Chen, H.; Yang, L. Effects of feedstock type, production method, and pyrolysis temperature on biochar and hydrochar properties. *Chem. Eng. J.* **2014**, *240*, 574–578. [CrossRef]
37. Jeguirim, M.; Chouchène, A.; Réguillon, A.F.; Trouvé, G.; Le Buzit, G. A new valorisation strategy of olive mill wastewater: Impregnation on sawdust and combustion. *Resour. Conserv. Recycl.* **2012**, *59*, 4–8. [CrossRef]
38. Zhang, B.; Heidari, M.; Regmi, B.; Salaudeen, S.; Arku, P.; Thimmannagari, M.; Dutta, A. Hydrothermal carbonization of fruit wastes: A promising technique for generating hydrochar. *Energies* **2018**, *11*, 2022. [CrossRef]
39. Yay, A.S.E.; Birinci, B.; Açıkalın, S.; Yay, K. Hydrothermal carbonization of olive pomace and determining the environmental impacts of post-process products. *J. Clean. Prod.* **2021**, *315*, 128087.
40. Chen, J.; Wang, P.; Ding, L.; Yu, T.; Leng, S.; Chen, J.; Fan, L.; Li, J.; Wei, L.; Li, J.; et al. Journal of Analytical and Applied Pyrolysis The comparison study of multiple biochar stability assessment methods. *J. Anal. Appl. Pyrolysis* **2021**, *156*, 105070. [CrossRef]

41. Jiang, L.; Hu, S.; Xiang, J.; Su, S.; Sun, L.; Xu, K.; Yao, Y. Bioresource Technology Release characteristics of alkali and alkaline earth metallic species during biomass pyrolysis and steam gasification process. *Bioresour. Technol.* **2012**, *116*, 278–284.
42. El-Bassi, L.; Azzaz, A.A.; Jellali, S.; Akrout, H.; Marks, E.A.N.; Ghimbeu, C.M.; Jeguirim, M. Application of olive mill waste-based biochars in agriculture: Impact on soil properties, enzymatic activities and tomato growth. *Sci. Total Environ.* **2021**, *755*, 142531. [CrossRef]
43. Jian, X.; Zhuang, X.; Li, B.; Xu, X.; Wei, Z.; Song, Y.; Jiang, E. Comparison of characterization and adsorption of biochars produced from hydrothermal carbonization and pyrolysis. *Environ. Technol. Innov.* **2018**, *10*, 27–35. [CrossRef]
44. Mahdi, Z.; El Hanandeh, A.; Yu, Q. Influence of Pyrolysis Conditions on Surface Characteristics and Methylene Blue Adsorption of Biochar Derived from Date Seed Biomass. *Waste Biomass Valoriz.* **2017**, *8*, 2061–2073. [CrossRef]
45. Ahmed, A.; Abu Bakar, M.S.; Hamdani, R.; Park, Y.K.; Lam, S.S.; Sukri, R.S.; Hussain, M.; Majeed, K.; Phusunti, N.; Jamil, F.; et al. Valorization of underutilized waste biomass from invasive species to produce biochar for energy and other value-added applications. *Environ. Res.* **2020**, *186*, 109596. [CrossRef]
46. Chouchene, A.; Jeguirim, M.; Favre-Reguillon, A.; Trouvé, G.; Le Buzit, G.; Khiari, B.; Zagrouba, F. Energetic valorisation of olive mill wastewater impregnated on low cost absorbent: Sawdust versus olive solid waste. *Energy* **2012**, *39*, 74–81. [CrossRef]
47. Lucian, M.; Volpe, M.; Gao, L.; Piro, G.; Goldfarb, J.L.; Fiori, L. Impact of hydrothermal carbonization conditions on the formation of hydrochars and secondary chars from the organic fraction of municipal solid waste. *Fuel* **2018**, *233*, 257–268. [CrossRef]
48. Atallah, E.; Kwapinski, W.; Ahmad, M.N.; Leahy, J.J.; Al-Muhtaseb, A.H.; Zeaiter, J. Hydrothermal carbonization of olive mill wastewater: Liquid phase product analysis. *J. Environ. Chem. Eng.* **2019**, *7*, 102833. [CrossRef]
49. Volpe, M.; Fiori, L. From olive waste to solid biofuel through hydrothermal carbonisation: The role of temperature and solid load on secondary char formation and hydrochar energy properties. *J. Anal. Appl. Pyrolysis* **2017**, *124*, 63–72. [CrossRef]
50. Zhao, S.X.; Ta, N.; Wang, X.D. Effect of Temperature on the Structural and Physicochemical Properties of Biochar with Apple Tree Branches as Feedstock Material. *Energies* **2017**, *10*, 1293. [CrossRef]
51. Jeguirim, M.; Trouvé, G. Pyrolysis characteristics and kinetics of Arundo donax using thermogravimetric analysis. *Bioresour. Technol.* **2009**, *100*, 4026–4031. [CrossRef]
52. Gallifuoco, A.; Taglieri, L.; Scimia, F.; Papa, A.A. Biomass and Bioenergy New insights into the evolution of solid and liquid phases during hydrothermal carbonization of lignocellulosic biomasses. *Biomass Bioenergy* **2019**, *121*, 122–127. [CrossRef]
53. Biller, P.; Ross, A.B. Production of biofuels via hydrothermal conversion. In *Handbook of Biofuels Production*; Elsevier: Amsterdam, The Netherlands, 2016; pp. 509–547. ISBN 9780081004562.
54. Weisenberger, M.C.; Burgess, J.; Schobert, H.H.; Hower, J.C.; Mountain, B. Thermal properties of Pennsylvania anthracite. *Fuel* **2020**, *266*, 117101. [CrossRef]
55. Wang, C.; Zhu, X.; Liu, X.; Lv, Q.; Zhao, L.; Che, D. Correlations of chemical properties of high-alkali solid fuels: A comparative study between Zhundong coal and biomass. *Fuel* **2018**, *211*, 629–637. [CrossRef]
56. Li, L.; Hale, M.; Olsen, P.; Berge, N.D. Using liquid waste streams as the moisture source during the hydrothermal carbonization of municipal solid wastes. *Waste Manag.* **2014**, *34*, 2185–2195. [CrossRef]
57. Magalh, D.; Gürel, K.; Matsakas, L.; Christakopoulos, P.; Pisano, I.; Leahy, J.J.; Kazanç, F.; Trubetskaya, A. Prediction of yields and composition of char from fast pyrolysis of commercial lignocellulosic materials, organosolv fractionated and torrefied olive stones. *Fuel* **2021**, *289*, 119862. [CrossRef]
58. Sangchoom, W.; Mokaya, R. Valorization of Lignin Waste: Carbons from Hydrothermal Carbonization of Renewable Lignin as Superior Sorbents for CO_2 and Hydrogen Storage. *ACS Sustain. Chem. Eng.* **2015**, *3*, 1658–1667. [CrossRef]
59. Volpe, M.; Goldfarb, J.L.; Fiori, L. Hydrothermal carbonization of Opuntia ficus-indica cladodes: Role of process parameters on hydrochar properties. *Bioresour. Technol.* **2018**, *247*, 310–318. [CrossRef]
60. Zhao, L.; Cao, X.; Mašek, O.; Zimmerman, A. Heterogeneity of biochar properties as a function of feedstock sources and production temperatures. *J. Hazard. Mater.* **2013**, *256–257*, 1–9. [CrossRef] [PubMed]
61. Vieira, F.R.; Romero Luna, C.M.; Arce, G.L.A.F.; Ávila, I. Optimization of slow pyrolysis process parameters using a fixed bed reactor for biochar yield from rice husk. *Biomass Bioenergy* **2020**, *132*, 105412. [CrossRef]
62. Teh, Y.Y.; Lee, K.T.; Chen, W.H.; Lin, S.C.; Sheen, H.K.; Tan, I.S. Dilute sulfuric acid hydrolysis of red macroalgae Eucheuma denticulatum with microwave-assisted heating for biochar production and sugar recovery. *Bioresour. Technol.* **2017**, *246*, 20–27. [CrossRef]
63. Zhao, C.; Jiang, E.; Chen, A. Volatile production from pyrolysis of cellulose, hemicellulose and lignin. *J. Energy Inst.* **2017**, *90*, 902–913. [CrossRef]
64. Azzaz, A.A.; Jellali, S.; Jeguirim, M.; Bousselmi, L.; Bengharez, Z.; Akrout, H. Optimization of a cationic dye desorption from a loaded-lignocellulosic biomass: Factorial design experiments and investigation of mechanisms. *Comptes Rendus. Chim.* **2021**, *24*, 71–84. [CrossRef]
65. Pfersich, J.; Arauzo, P.J.; Lucian, M.; Modugno, P.; Titirici, M.M.; Fiori, L.; Kruse, A. Hydrothermal Conversion of Spent Sugar Beets into High-Value Platform Molecules. *Molecules* **2020**, *25*, 3914. [CrossRef]
66. Liang, J.; Liu, Y.; Zhang, J. Effect of Solution pH on the Carbon Microsphere Synthesized by Hydrothermal Carbonization. *Procedia Environ. Sci.* **2011**, *11*, 1322–1327. [CrossRef]
67. Ryu, J.; Suh, Y.-W.; Suh, D.J.; Ahn, D.J. Hydrothermal preparation of carbon microspheres from mono-saccharides and phenolic compounds. *Carbon N. Y.* **2010**, *48*, 1990–1998. [CrossRef]

68. Volpe, R.; Messineo, A.; Millan, M.; Volpe, M.; Kandiyoti, R. Assessment of olive wastes as energy source: Pyrolysis, torrefaction and the key role of H loss in thermal breakdown. *Energy* **2015**, *82*, 119–127. [CrossRef]
69. Zhang, S.; Sheng, K.; Yan, W.; Liu, J.; Shuang, E.; Yang, M.; Zhang, X. Bamboo derived hydrochar microspheres fabricated by acid-assisted hydrothermal carbonization. *Chemosphere* **2021**, *263*, 128093. [CrossRef]
70. Qatarneh, A.F.; Dupont, C.; Michel, J.; Simonin, L.; Beda, A.; Matei Ghimbeu, C.; Ruiz-Villanueva, V.; da Silva, D.; Piégay, H.; Franca, M.J. River driftwood pretreated via hydrothermal carbonization as a sustainable source of hard carbon for Na-ion battery anodes. *J. Environ. Chem. Eng.* **2021**, *9*, 106604. [CrossRef]
71. Basso, D.; Weiss-Hortala, E.; Patuzzi, F.; Castello, D.; Baratieri, M.; Fiori, L. Hydrothermal carbonization of off-specification compost: A byproduct of the organic municipal solid waste treatment. *Bioresour. Technol.* **2015**, *182*, 217–224. [CrossRef]
72. Jeguirim, M.; Goddard, M.L.; Tamosiunas, A.; Berrich-Betouche, E.; Azzaz, A.A.; Praspaliauskas, M.; Jellali, S. Olive mill wastewater: From a pollutant to green fuels, agricultural water source and bio-fertilizer. Biofuel production. *Renew. Energy* **2020**, *149*, 716–724. [CrossRef]
73. Igalavithana, A.D.; Choi, S.W.; Dissanayake, P.D.; Shang, J.; Wang, C.H.; Yang, X.; Kim, S.; Tsang, D.C.W.; Lee, K.B.; Ok, Y.S. Gasification biochar from biowaste (food waste and wood waste) for effective CO2 adsorption. *J. Hazard. Mater.* **2020**, *391*, 121147. [CrossRef] [PubMed]
74. Yoo, S.; Kelley, S.S.; Tilotta, D.C.; Park, S. Structural Characterization of Loblolly Pine Derived Biochar by X-ray Diffraction and Electron Energy Loss Spectroscopy. *ACS Sustain. Chem. Eng.* **2018**, *6*, 2621–2629. [CrossRef]
75. Guo, S.; Dong, X.; Wu, T.; Shi, F.; Zhu, C. Characteristic evolution of hydrochar from hydrothermal carbonization of corn stalk. *J. Anal. Appl. Pyrolysis* **2015**, *116*, 1–9. [CrossRef]
76. Sevilla, M.; Fuertes, A.B. The production of carbon materials by hydrothermal carbonization of cellulose. *Carbon N. Y.* **2009**, *47*, 2281–2289. [CrossRef]
77. Zhang, C.; Zhang, Z.; Zhang, L.; Li, Q.; Li, C.; Chen, G.; Zhang, S.; Liu, Q.; Hu, X. Evolution of the functionalities and structures of biochar in pyrolysis of poplar in a wide temperature range. *Bioresour. Technol.* **2020**, *304*, 123002. [CrossRef] [PubMed]
78. Chouchene, A.; Jeguirim, M.; Trouvé, G.; Favre-Reguillon, A.; Le Buzit, G. Combined process for the treatment of olive oil mill wastewater: Absorption on sawdust and combustion of the impregnated sawdust. *Bioresour. Technol.* **2010**, *101*, 6962–6971. [CrossRef] [PubMed]
79. Saha, N.; Saba, A.; Reza, M.T. Effect of hydrothermal carbonization temperature on pH, dissociation constants, and acidic functional groups on hydrochar from cellulose and wood. *J. Anal. Appl. Pyrolysis* **2019**, *137*, 138–145. [CrossRef]
80. Haddad, K.; Jeguirim, M.; Jellali, S.; Guizani, C.; Delmotte, L.; Bennici, S.; Limousy, L. Combined NMR structural characterization and thermogravimetric analyses for the assessment of the AAEM effect during lignocellulosic biomass pyrolysis. *Energy* **2017**, *134*, 10–23. [CrossRef]